Materials Research. 2019; 22(4): e20190320
DOI: http://dx.doi.org/10.1590/1980-5373-MR-2019-0320

Microstructural Evolution Due to One Thermal Cycle in a Superduplex Stainless Steel ASTM A890/A890M - Grade 6A in the As-Weld and Post-Weld Heat Treatment Conditions

***Clélia Ribeiro de Oliveira*[a]*, *Eloá Lopes Maia*[a], *Solange Tamara da Fonseca*[a], *Marcelo Martins*[b], *Julian Arnaldo Avila*[c], *Paulo Roberto Mei*[a]**

[a]*Universidade Estadual de Campinas - Unicamp, Rua Mendeleyev, 200, 13083-860. Campinas, SP, Brasil*
[b]*Centro Universitário Salesiano de São Paulo - UNISAL, Americana, Rua Dom Bosco, 100, 13466-327, Americana, SP, Brasil*
[c]*Universidade Estadual Paulista - UNESP, 13876-750, São João da Boa Vista, SP, Brasil*

Received: May 05, 2019; Revised: May 21, 2019; Accepted: June 03, 2019

During welding of the superduplex stainless steels are exposed to thermal cycles, allowing precipitation of deleterious phases as well as unbalance as the ferrite and austenite phases. This work analyzed the microstructural changes taking place on a plate ASTM A890/A890M - grade 6A steel submitted to arc welding one welding of pass conducted on a flat surface using coated electrode Zeron®100, in the as welded and post-welded heat treatment conditions. Microstructural characterization in the regions base metal, heat affected zone, and fusion zone were conducted by optical microscopy, scanning electron microscopy and X-ray diffraction. The post-weld heat treatment in the fusion zone changed the ferrite/austenite volumetric fraction from 59/41 to 52/48. Cr, Mo and Ni distributions in the fusion zone were altered after the post-weld heat treatment, with the concentration ratio ferrite/austenite being around 1.0; 1.1 and 0.9 to 1.1; 1.4 and 0.7, respectively. In addition, hardness reduced from 300 to 270 $HV_{0.3}$ at the fusion zone.

Keywords: *superduplex stainless steel, ASTM A890/A890M, post-weld heat treatment.*

1. Introduction

The superduplex stainless steels (SDSS) depict a microstructure composed of austenite (γ) and ferrite (δ), normally with a 1:1 ratio[1-3]. The formation of these two phases is determined by the preferential partitioning of the alloying elements, ferrite, and austenite phases, especially the Cr, Ni and Mo[4]. Cr and Mo enrich ferrite, while Ni and N are concentrated in austenite[5,6]. These materials show a compelling combination of excellent corrosion resistance and high mechanical properties[1,7]. For example, SDSS steels belonging to the Fe-Cr-Ni system present outstanding corrosion resistance, with pitting resistance equivalent number (PREN) above 40[1,3], with Cr and Mo contents around 25-27% and 3-4.5 %, respectively[6].

High temperature changes the morphology of the microstructure of SDSS steels, as well as the partitioning of alloying elements, which affects the mechanical and corrosion properties of the heat-affected zone (HAZ)[8] and fusion zone (FZ). The greater the presence of alloying elements in these steels, the greater the probability of forming deleterious phases, such as sigma, when the material is exposed to thermal treatments or welding thermal cycles[9].

Some authors have reported that in the HAZ may precipitate Cr_2N, χ, and σ at different typical temperatures[10,11]. In these regions, high or very low heat input may be unfavorable for phase adjustment, under high heat input conditions may result in precipitation of intermetallic phases, and when low heat input conditions are presented, may raise the ferrite content[11]. A heat input of 0.5 to 2.5 kJ/mm is recommended for 25% Cr[12].

Partitioning of alloying element and partition coefficient are dependent on cooling rates, which in slower cooling rates can diffuse completely elements that stabilizes austenite (N, Ni) of the ferrite matrix to austenite precipitates[6,13]. The degree of partitioning of the alloying elements between the phases δ and γ calculated by the partition coefficient greatly affects the corrosion resistance of the SDSS[2,5,8]. Several authors have reported that post-welded heat treatment (PWHT) can improve corrosion resistance properties[14-17], due to the homogenization of phases ratio. The PREN is affected by the partition of the alloying elements, the ferrite tends to increase with temperature and the Cr and Mo gets more diluted in this phase[17-19].

The objective of this work is to evaluate the effect of one welding pass conducted on a flat surface of superduplex stainless steel and to verify the effect on the microstructure of the welded joints. The steel analyzed in this research was obtained in sand casting, it is regulated by ASTM A890/A890M with grade 6A specification. The joints were evaluated in the as-welded and PWHT conditions. The analyzes were performed in the regions base metal (BM), heat-affected zone (HAZ) and fusion zone (FZ). The partition coefficient, phase

*e-mail: clelia.rib@hotmail.com.

morphology, microhardness and X-ray diffraction (XRD) were evaluated in the different conditions.

2. Experimental Procedure

Plates with dimensions of 360 mm x 110 mm x 40 mm of a ASTM A890/A890M grade 6A[20] steel were studied. The steel was prepared in a 60 Hz Vacuum Induction Melting (VIM) furnace and poured in plate shaped sand molds bounded with phenolic-urethane resin. After solidification and demolding, the plates were then heated for 4 hours at a temperature of 1140 °C to adjust ferrite/austenite balance recommended by the ASTM A890/A890M standard[20].

The welding parameters of the company that supplied the material. Bead-on-plate pass was conducted using shielded metal arc welding (SMAW) process, with voltage 20-25 V and current 100-130 A, heat input 1.3 kJ/mm and speed 1.23 mm/s. The coated electrode was the Zeron®100, whose chemical composition is similar to the steel used in this work, as shown in Table 1. After welding, the plate was sectioned in two parts, with one of them subjected to a PWHT at 1150 °C for 2 h 45 min and subsequent cooling in water. This procedure aimed to approximate the amount of ferrite and austenite to a 1:1 ratio.

For microstructural characterization, samples of the area of interest, such as BM, HAZ and FZ, transversal to the weld, were grinded using sandpaper with grit size of 180 to 1200, and polished with diamond paste 6, 3 and 1 µm. To revealing the microstructure of the samples, electrolyte etching was conducted with 3 volts for 15 seconds in a 20% aqueous solution of NaOH.

The images were obtained by light optical microscope (LOM) and by secondary electron detector coupled to a scanning electron microscope (SEM). The chemical analysis was performed by Energy Dispersion X-Ray Spectroscopy (EDS). The partition coefficients (K) was calculated by Equation 1, where C_δ is the concentration of ferrite and C_γ is the concentration of austenite[21].

$$K = C_\delta / C_\gamma \qquad \text{Equation 1}$$

Phase quantification in the regions of the BM, HAZ and FZ under the as-welded and PWHT conditions was performed by image analysis according to ASTM E1245 standard[22]. The phase identification was performed by X-ray diffraction (XRD) technique and a cobalt (CoKα1) source with a wavelength length of 1,789 Å, 40 kV, 40 mA and step of 0.02 °/min. The Vickers (HV) hardness measurements conducted with a load of 2.94 N (0.300 kgf) and a loading time of 15 seconds using the ASTM E384 standard[23].

3. Results

Figure 1a show the cross-section and the transition between the BM and FZ weld bead produced on SDSS plate. From images, three distinct regions are depicted, the fusion zone (FZ), the heat-affected zone (HAZ) and the base metal (BM). A clear difference in the weld bead as-welded and PWHT can be observed in the Figure 1d-e. The Figure 2 shows the volumetric fraction of the ferrite and austenite phases in the BM and FZ, in the as-welded and PWHT conditions.

In the microstructural analysis, it was observed that BM depicted austenite islands precipitated in ferrite matrix, as shown in Figure 1b, with a ferrite/austenite fraction of 47/53 shown in Figure 2. The post-weld heat treatment showed little change in the structure of BM as shown in Figure 1c, with a ferrite/austenite ratio of 49/51. The change was not significant, since the BM had already been heat-treated after the plate was made, to balance the volumetric fraction of ferrite and austenite. In the transition region between the BM and the FZ a transition region, called the HAZ, the precipitation of ferrite occurs within the pre-existing austenite islands as shown in Figure 1d. In multipass welds the austenite dissolves during heating to form the ferrite and during cooling the austenite precipitates, especially, in the contours of ferrite grains. In HAZ, however, austenite does not dissolve completely, so it is observed that the morphology at the interface between ferrite and austenite is partially altered[24].

After welding, FZ presented a ferritic matrix with acicularized austenitic structure (Widsmanstätten type)[25] and precipitated in the contour and inside of the ferritic grain, see Figure 1f. This acicularized structure is typical in regions that melt during welding and which solidify rapidly. Rapid solidification inhibited the growth of austenite from the ferrite. In the solidification of this alloy the first phase to be formed from the liquid is the ferrite, as can be observed in 70Fe/25Cr/5Ni steel[26], whose basic chemical composition is close to the steel used in this work.

The post-welded heat treatment in the FZ favored austenite growth and the ferrite/austenite volumetric fraction ratio approached the balance, from 59/41 to 52/48[1,2] as shown in

Table 1. Chemical composition and PREN of ASTM A890/A890M - Grade 6A steel and Zeron®100 electrode (wt%).

	C	Mn	Si	P	S	Cr	Ni	Mo	Cu	W	N
6A	0.023	0.77	0.91	0.025	0.005	25.13	8.22	3.53	0.89	0.67	0.29
Zeron®100	0.028	0.79	0.72	0.029	0.006	25.1	8.06	4.19	0.42	0.44	0.26
					6A				Zeron®100 electrode		
PREN*					41.4				43.1		

*PREN = %Cr+3.3%Mo+16%N≥40 (% by weight).

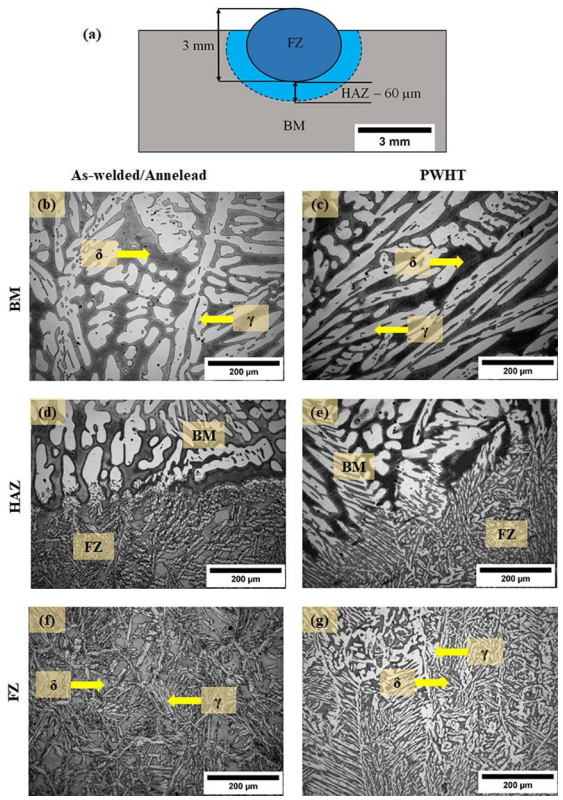

Figure 1. Macrostructure of the bead-on-plate, transversal view (a). Microstructures observed in the BM, HAZ and FZ in the conditions: as-welded/annealed (b-d-f) and PWHT (c-e-g). Electrolytic etching with 20% NaOH. LOM.

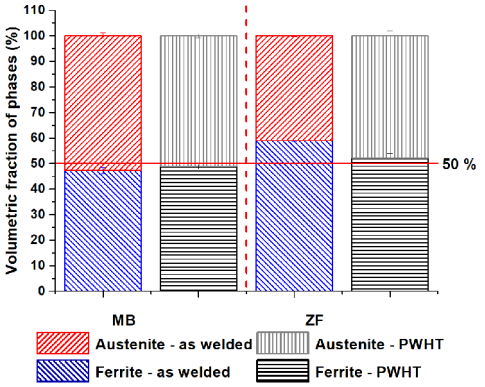

Figure 2. Volumetric fraction of the ferrite and austenite phases in the BM and FZ, in the conditions as-welded and PWHT.

Figure 2. The growth of austenite with PWHT also reduced its acicular shape somewhat according Figure 1f.

As shown in Table 2 and Figure 3, Cr, Mo and Ni distributions in BM were not significantly altered after PWHT, with the ferrite/austenite concentration ratio being around 1.1, 1.6 and 0.7 respectively. These data are consistent with literature, which indicate a ferrite/austenite ratio greater than 1 for ferrite stabilizing elements such as Cr and Mo; and less than 1 for stabilized austenite elements, such as Ni[2,5,13,21,27]. However, in the FZ, which was cooled rapidly, with PWHT there was diffusion of Cr and Mo from austenite to ferrite and from Ni in the opposite direction.

The PREN (%Cr+3.3%Mo+16%N) of the ferrite and austenite phases is shown in Table 2, as well as the overall value **($(PREN_\delta + PREN_\gamma)/2$)**, the nitrogen value (% wt) of 0.29 for the BM and 0.26 for the FZ, values that are available in Table 1, since this chemical element is light to be detected by the EDS. It was observed that austenite presents lower values of PREN in BM, for both conditions. However, in FZ in the as-welded condition the values were equivalent, but in the condition with PWHT obtained smaller value. The PREN in FZ after PWHT was equivalent to BM in both conditions. In thermally treated materials PREN tends to increase in the ferrite phase and decrease in the austenite phase[28]. This condition tends to improve the resistance to pitting corrosion since the ferrite is more susceptible to corrosion and in this state, this phase presents the best conditions[13].

Table 2. Concentration of Cr, Mo and Ni (% by weight) of the ferrite and austenite phases present in the BM and FZ, in the conditions as-welded and PWHT. Concentration ratio between ferrite and austenite. Data obtained with SEM/EDS.

PWHT	Phase	Cr		Mo		Ni		$PREN_{\delta-\gamma}$	
		BM	FZ	BM	FZ	BM	FZ	BM	FZ
No	Ferrite	27.4 ± 0.3	26.1±0.2	4.2±0.2	3.6±0.2	6.6±0.2	9.0±0.2	45.9	42.1
	Austenite	24.8 ± 0.3	25.7±0.3	2.7±0.2	3.2±0.3	9.6±0.2	9.7±0.4	38.4	40.4
	δ/γ	1.1	1.0	1.6	1.1	0.7	0.9		
	$PREN_{BM}$	$PREN_{BM} = (PREN_\delta + PREN_\gamma)/2 = 42.1$							
	$PREN_{FZ}$	$PREN_{FZ} = (PREN_\delta + PREN_\gamma)/2 = 41.3$							
Yes	Ferrite	27.5± 0.2	27.9±0.4	4.4±0.2	4.4±0.1	6.5±0.3	6.7±0.2	46.7	46.6
	Austenite	24.6± 0.3	25.0±0.5	2.8±0.2	3.1±0.3	9.8±0.3	10.1±0.4	38.5	39.4
	δ/γ	1.1	1.1	1.6	1.4	0.7	0.7		
	$PREN_{BM}$	$PREN_{BM} = (PREN_\delta + PREN_\gamma)/2 = 42.6$							
	$PREN_{FZ}$	$PREN_{FZ} = (PREN_\delta + PREN_\gamma)/2 = 43.0$							

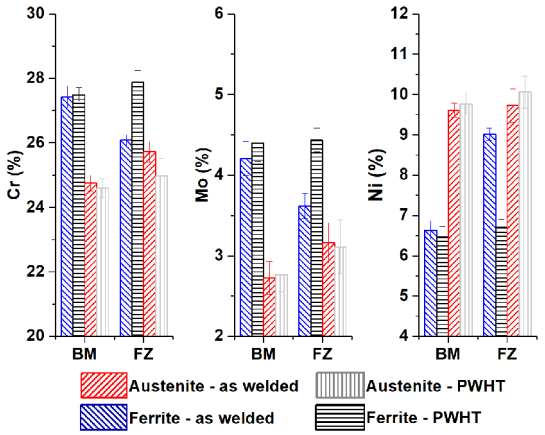

Figure 3. Concentration of Cr, Mo and Ni (weight %) of the ferrite and austenite phases present in the BM and FZ in the condition as-welded and PWHT. Data obtained by SEM/EDS.

In the XRD analysis, only the ferrite and austenite peaks as shown in Figure 4 were detected in the BM and FZ regions as-welded and PWHT. The ferrite peaks (body centered cubic - BCC structure) occurred in the {110}, {200}, {211}, {220} planes and those of the austenite (face centered cubic - FCC structure) planes {111}, {200}, {220}, {311}, {222}. The austenite peaks became more evident in the condition after PWHT, it is noticed that in the annealed BM the present peaks of both phases are balanced indicating that there is volumetric balance of the phases. It was also observed that in the FZ as-welded ferrite peaks prevailed, this result is coherent with the volumetric fractions of the present phases, because in this condition it is common that these steels have higher ferrite contents.

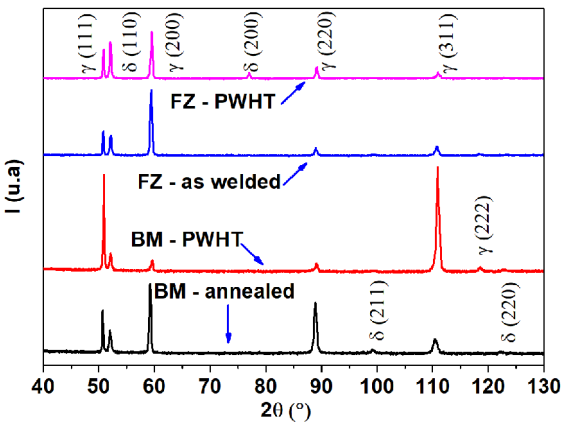

Figure 4. X-ray diffraction in the BM and FZ regions, in as-welded and PWHT conditions.

The hardness in the BM remained at 250 $HV_{0.3}$ after the PWHT, see Figure 5, this is justified because the heat treatment did not significantly alter the volumetric fractions of the phases and nor the microstructure thereof. In the FZ, however, as the fast solidification acicularized the austenite and raised the volumetric fraction of the ferrite, which is a phase of greater hardness than the austenite, the hardness of the region increased to 300 $HV_{0.3}$. The PWHT in the FZ softened the acicularization of austenite and increased its volumetric fraction from 41 to 48%, at the expense of the ferrite consumption, facts that resulted in a reduction of the hardness of the steel to 270 $HV_{0.3}$.

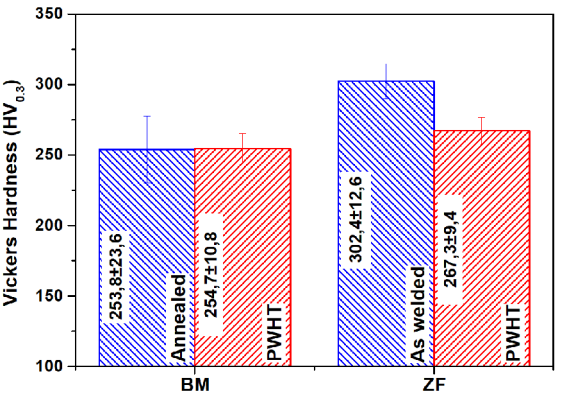

Figure 5. Vickers hardness in the BM and FZ, in the conditions as-welded (FZ), annealed (BM) and PWHT.

The hardness reduction occurs because the austenite has a lower hardness than the ferrite with values of 266 ± 9 $HV_{0.3}$ and 301 ± 13 $HV_{0.3}$, respectively, results obtained in BM in annealed condition. The higher presence of Cr and Mo in the ferrite phase increases the hardness of the same. In addition, ferrite has less slip systems than austenite at room temperature[29].

4. Discussion

The partition of the elements between austenite and ferrite is driven by the phenomenon of diffusion, i.e., the partition coefficient depends on the cooling rate. In slow cooling there is an excellent partition of the elements between the two phases, based on the thermodynamic characteristics of each element. When the cooling is fast, the diffusion is inhibited, producing austenite and ferrite of homogeneous composition, leading to partition coefficients with very high values close to 1.

At high temperatures the Ni tends to be concentrated also in the ferrite phase, the behavior observed in the FZ[1]. The partition coefficient of the Cr alloy element for all conditions was around 1, slightly stabilizing the ferrite phase[2]. The alloying element Mo preferably stabilizes the ferrite phase, but its concentration is decreased in this phase in the FZ of the as-welded condition, due to the cooling conditions, not having time for diffusion in the ferrite phase and being part retained austenite. High cooling rates induced by the welding process leads to significant variation in the grain size, orientation and shape in the FZ microstructures when

compared to BM, as also reported in previous studies[12]. The PWHT enabled the partitioning of the alloying elements and changed/modified 1.0; 1.1 and 0.9 to 1.1; 1.4 and 0.7 for chemical elements: Cr, Mo and Ni, respectively.

Hardness in the FZ was the highest and even after PWHT was higher than BM, since the welding can cause the tension induced hardening during the solidification of the weld, fast thermal heating and cooling cycle, residual tension and higher concentrations of elements of alloys trapped in the crystalline lattice of the phases[30], which ends increasing hardness in the matrix.

In these steels the ferrite presents a higher hardness than austenite because it contains higher Cr and Mo contents in its composition[12] and because its volumetric fraction was higher in the FZ before the PWHT and there was still a higher Ni absorption, the hardness tends to be higher in these regions. Moreover, BCC crystal (ferrite) structures have less slip systems than the crystalline FCC structure at room temperature[29]. Austenite has much more deformation modes, such as dislocation slips, shear banding and phase transformations, while the ferrite undergoes deformations by dislocation slips on many operating slip systems[30-34].

5. Conclusions

Based on the materials and results of the experimental techniques used, it is possible to conclude that:

- The PWHT in the fusion zone changed the ferrite/austenite volumetric fraction from 59/41 to 52/48, The partition coefficient ratio ferrite/austenite of the chemical elements Cr, Mo and Ni being around 1.0; 1.1 and 0.9 to 1.1; 1.4 and 0.7, respectively after PWHT. This result confirms that Cr and Mo tend to stabilize the ferrite phase and Ni the austenite phase, since PWHT allowed the diffusion of these alloying elements.
- PREN in FZ after PWHT was equivalent to BM in both conditions. In thermally treated materials PREN tends to increase in the ferrite phase and decrease in the austenite phase;
- The PWHT balanced the phases proportions produced after welding. Likewise, alloying elements partition and microhardness equilibrium was favored by the PWHT.
- Austenite and ferrite were the only phases found by the XRD analysis, however the intensity or the appearance of the peaks showed that there is a certain tendency in the formation of the phases, because in the conditions with PWHT the peaks are equivalent and on the other hand, in the as-welded FZ the peaks of ferrite are more evident.
- The fusion zone presented a refined austenite grains, while BM depicts austenite plates. This characteristic was observed in the two conditions, although the adjustment of the phases after the PWHT occurred to a more proportion close to 1:1 ratio.

6. Acknowledgment

The authors are grateful to Conselho Nacional de Desenvolvimento Cientifico e Tecnológico (CNPq) - process number 142260/2016-9, FEM/UNICAMP for the facilities (SEM Zeiss EVO-MA15) and SULZER BRASIL SA for supplying the ASTM A890/A890M grade 6A steel. This research was supported by LNNano - Brazilian Nanotechnology National Laboratory, CNPEM/MCTIC, proposals: No. 18519 and No. 19209, for the use of DRX-P (X-ray diffractometer PANalytical X'Pert PRO MRD XL System), SEM and the durometer model Future-Tech FV 800.

7. References

1. Charles J. Duplex stainless steels, a review after DSS'07 in Grado. *Revue de Métallurgie*. 2008;105(3):155-171.
2. Zhang Z, Jing H, Xu L, Han Y, Zhao L, Zhang J. Influence of microstructure and elemental partitioning on pitting corrosion resistance of duplex stainless steel welding joints. *Applied Surface Science*. 2017;394:297-314. DOI: 10.1016/j.apsusc.2016.10.047
3. Nilsson JO. Super duplex stainless steels. *Materials Science and Technology*. 1992;8(8):685-700. DOI: http://dx.doi.org/10.1179/mst.1992.8.8.685
4. Jorge Júnior AM, Reis GS, Balancin O. Influence of the microstructure on the plastic behaviour of duplex stainless steels. *Materials Science and Engineering: A*. 2011;528(6):2259-2264. DOI: 10.1016/j.msea.2010.11.087
5. Cortie MB, Potgieter JH. The effect of temperature and nitrogen content on the partitioning of alloy elements in duplex stainless steels. *Metallurgical Transactions A*. 1991;22(10):2173-2179.
6. Weber L, Uggowitzer PJ. Partitioning of chromium and molybdenum in super duplex stainless steels with respect to nitrogen and nickel content. *Materials Science and Engineering: A*. 1998;242(1-2):222-229. DOI: 10.1016/S0921-5093(97)00521-2
7. Gunn RN, ed. Duplex Stainless Steels: Microstructure, properties and applications. Cambridge: Abington Publishing; 2003.
8. Muthupandi V, Bala Srinivasan P, Seshadri SK, Sundaresan S. Effect of weld metal chemistry and heat input on the structure and properties of duplex stainless steel welds. *Materials Science and Engineering: A*. 2003;358(1-2):9-16. DOI: 10.1016/S0921-5093(03)00077-7
9. Nilsson JO, Wilson A. Influence of isothermal phase transformations on toughness and pitting corrosion of super duplex stainless steel SAF 2507. *Materials Science and Technology*. 1993;9(7):545-554. DOI: 10.1179/mst.1993.9.7.545
10. Deng B, Wang Z, Jiang Y, Sun T, Xu J, Li J. Effect of thermal cycles on the corrosion and mechanical properties of UNS S31803 duplex stainless steel. *Corrosion Science*. 2009;51(12):2969-2975. DOI: 10.1016/j.corsci.2009.08.015

11. Kotecki DJ. Some pitfalls in welding of duplex stainless steels. *Soldagem & Inspeção*. 2010;15(4):336-343. DOI: 10.1590/S0104-92242010000400011

12. Vinoth Jebaraj A, Ajaykumar L, Deepak CR, Aditya KVV. Weldability, machinability and surfacing of commercial duplex stainless steel AISI2205 for marine applications - A recent review. *Journal of Advanced Research*. 2017;8(3):183-199. DOI: 10.1016/j.jare.2017.01.002

13. de Souza EC, Rossiti SM, Fortulan CA, Rollo JMDA. Influence of Ferrite Phase Content on the Electrochemical Properties of Duplex Stainless Steels. *Materials Research*. 2017;20(1):21-29.

14. Prabakaran MP, Kannan GR. Optimization of laser welding process parameters in dissimilar joint of stainless steel AISI316/AISI1018 low carbon steel to attain the maximum level of mechanical properties through PWHT. *Optics & Laser Technology*. 2019;112:314-322. DOI: 10.1016/j.optlastec.2018.11.035

15. Cao XY, Ding XF, Lu YH, Zhu P, Shoji T. Influences of Cr content and PWHT on microstructure and oxidation behavior of stainless steel weld overlay cladding materials in high temperature water. *Journal of Nuclear Materials*. 2015;467(Pt 1):32-41. DOI: 10.1016/j.jnucmat.2015.09.015

16. Pilhagen J, Sieurin H, Sandström R. Fracture toughness of a welded super duplex stainless steel. *Materials Science and Engineering: A*. 2014;606:40-45. DOI: http://dx.doi.org/10.1016/j.msea.2014.03.049

17. Zhang Z, Wang Z, Jiang Y, Tan H, Han D, Guo Y, et al. Effect of post-weld heat treatment on microstructure evolution and pitting corrosion behavior of UNS S31803 duplex stainless steel welds. *Corrosion Science*. 2012;62:42-50. DOI: 10.1016/j.corsci.2012.04.047

18. Jiang Y, Tan H, Wang Z, Hong J, Jiang L, Li J. Influence of Cr_{eq}/Ni_{eq} on pitting corrosion resistance and mechanical properties of UNS S32304 duplex stainless steel welded joints. *Corrosion Science*. 2013;70:252-259. DOI: 10.1016/j.corsci.2013.01.037

19. Tan H, Jiang Y, Deng B, Sun T, Xu J, Li J. Effect of annealing temperature on the pitting corrosion resistance of super duplex stainless steel UNS S32750. *Materials Caracterization*. Charact. 2009;60(9):1049-1054. DOI: 10.1016/j.matchar.2009.04.009

20. ASTM International. *ASTM A890/A890M - 13 - Standard Specification for Castings, Iron-Chromium-Nickel-Molybdenum Corrosion-Resistant, Duplex (Austenitic/Ferritic) for General Application*. West Conshohocken: ASTM International; 2013.

21. Atamert S, King JE. Elemental partitioning and microstructural development in duplex stainless steel weld metal. *Acta Metallurgica et Materialia*. 1991;39(3):273-285. DOI: 10.1016/0956-7151(91)90306-L

22. ASTM International. *ASTM E1245 - Standard Practice for Determining the Inclusion or Second-Phase Constituent Content of Metals by Automatic Image Analysis*. West Conshohocken: ASTM International; 1999.

23. ASTM International. *ASTM E384-11e1 - Standard Test Method for Knoop and Vickers Hardness of Materials*. West Conshohocken: ASTM International; 2011.

24. Guo Y, Sun T, Hu J, Jiang Y, Jiang L, Li J. Microstructure evolution and pitting corrosion resistance of the Gleeble-simulated heat-affected zone of a newly developed lean duplex stainless steel 2002. *Journal of Alloys and Compounds*. 2016;658:1031-1040. DOI: 10.1016/j.jallcom.2015.10.218

25. Villalobos-Vera DI, Mendoza-Bravo I. Microstructural Transformation in a Root Pass of Superduplex Stainless Steel Multipass Welding. *Materials Research*. 2017;20(2):303-307.

26. Atamert S, King JE. Super duplex stainless steels Part 1 Heat affected zone microstructures. *Materials Science and Technology*. 1992;8(10):896-912.

27. Wan J, Lou Y, Ruan H. The partition coefficient of alloying elements and its influence on the pitting corrosion resistance of 15Cr-2Ni duplex stainless steel. *Corrosion Science*. 2018;139:13-20. DOI: 10.1016/j.corsci.2018.04.038

28. Sun L, Sun Y, Liu Y, Dai N, Li J, Jiang Y. Effect of annealing temperature on pitting behavior and microstructure evolution of hyper-duplex stainless steel 2707. *Materials and Corrosion*. 2019;1-11. DOI: 10.1002/maco.201910801

29. Warren AD, Griffiths IJ, Harniman RL, Flewitt PEJ, Scott TB. The role of ferrite in Type 316H austenitic stainless steels on the susceptibility to creep cavitation. *Materials Science and Engineering: A*. 2015;635:59-69. DOI: 10.1016/j.msea.2015.03.048

30. Ameri A, Quadir Z, Ashraf M, Logos C, Escobedo-Diaz J. Effects of load partitioning and texture on the plastic anisotropy of duplex stainless steel alloys under quasi-static loading conditions. *Materials Science and Engineering: A*. 2019;752:24-35. DOI: 10.1016/j.msea.2019.02.090

31. Jeong CU, Heo YU, Choi JY, Woo W, Choi SH. A study on the micromechanical behaviors of duplex stainless steel under uniaxial tension using ex-situ experimentation and the crystal plasticity finite element method. *International Journal of Plasticity*. 2015;75:22-38. DOI: 10.1016/j.ijplas.2015.07.005

32. Herrera C, Ponge D, Raabe D. Design of a novel Mn-based 1 GPa duplex stainless TRIP steel with 60% ductility by a reduction of austenite stability. *Acta Materialia*. 2011;59(11):4653-4664. DOI: 10.1016/j.actamat.2011.04.011

33. Li Y, Li W, Hu JC, Song HM, Jin XJ. Compatible strain evolution in two phases due to epsilon martensite transformation in duplex TRIP-assisted stainless steels with high hydrogen embrittlement resistance. *International Journal of Plasticity*. 2017;88:53-69. DOI: 10.1016/j.ijplas.2016.09.012

34. Raabe D. Simulation of rolling textures of b.c.c. metals considering grain interactions and crystallographic slip on {110}, {112} and {123} planes. *Materials Science and Engineering: A*. 1995;197(1):31-37. DOI: 10.1016/0921-5093(94)09770-4